PCCP



View Article Online **PAPER**



Cite this: Phys. Chem. Chem. Phys., 2022. 24. 23699

Non-Aufbau orbital ordering and spin density modulation in high-spin donor-acceptor conjugated polymers†

Md Abdus Sabuj, D Obinna Muoh, Md Masrul Huda and Neeraj Rai D*

High-spin ground-state organic materials with unique spin topology can significantly impact molecular magnetism, spintronics, and quantum computing devices. However, strategies to control the spin topology and alignment of the unpaired spins in different molecular orbitals are not well understood. Here, we report modulating spin distribution along the molecular backbone in high-spin ground-state donor-acceptor (D-A) conjugated polymers. Density functional theory calculations indicate that substitution of different heteroatoms (such as C, Si, N, and Se) alters the aromatic character in the thiadiazole unit of the benzobisthiadiazole (BBT) acceptor and modulates the oligomer length to result in high-spin triplet ground-state, orbital and spin topology. The C, Si, and Se atom substituted polymers show a localized spin density at the two opposite ends of the polymers. However, a delocalized spin distribution is observed in the N substituted polymer. We find that the hybridization (sp³ vs. sp²) of the substituent atom plays an important role in controlling the electronic structure of these materials. This study shows that atomistic engineering is an efficient technique to tune the spin topologies and electronic configurations in the high-spin ground-state donor-acceptor conjugated polymers, compelling synthetic targets for room-temperature magnetic materials.

Received 24th May 2022, Accepted 8th September 2022

DOI: 10.1039/d2cp02355e

rsc.li/pccp

1 Introduction

Open-shell organic semiconductors (OSCs) with a high-spin $(S \ge 1)$ ground-state and localized spin topology defy the perpetual notion of spin-pairing as in chemical bonds and are widely utilized in numerous emerging optoelectronic and magnetic applications. OSCs with two (diradicals) or more number of unpaired electrons (polyradicals) have unique optical, electronic, spin-transport, and magnetic properties, making them suitable for potential application in organic photovoltaics, solar cells, charge-storage devices, organic spintronics, and magnetic materials. 1-9 Research endeavors are mostly directed towards finding novel organic high-spin state molecules 10-17 to understand the core mechanism of magnetism which may facilitate the development of new materials with improved optoelectronic and magnetic properties.5,18 However, the mechanism to control the spin distribution and alignment of unpaired electrons in molecular orbitals (MOs) is not well studied. 9,19-23

Dave C Swalm School of Chemical Engineering, and Center for Advanced Vehicular Systems, Mississippi State University, Mississippi State, Mississippi, 39762, USA. E-mail: neerajrai@che.msstate.edu; Fax: +1-662-325-2482; Tel: +1-662-325-0790 † Electronic supplementary information (ESI) available: Optimized ground-state geometric parameters, NICSiso(1) values, MO diagrams, spin density diagrams. See DOI: https://doi.org/10.1039/d2cp02355e

The unpaired electrons in open-shell OSCs can be in a spinpaired low-spin singlet (S = 0) ground-state or both spins can be aligned in a spin-parallel high-spin triplet (S = 1) state, overcoming the effect of double-spin polarization. 19,20,24 The relative preference for a low- and high-spin ground-state can be controlled by the electron distribution along the molecular backbone. 5,9,20,25,26 The closed-shell materials with a low-spin ground-state tend to accumulate the spin density at the core of the molecular backbone, 20 whereas the open-shell materials with a high-spin ground-state show either a delocalized 19,21 or an end localized orbital topology.20 However, spin-ordering at room temperature is controlled by the magnitude of spin localization, as observed in the edge-modified graphene nanoribbons (GNRs) or zigzag edge graphene nanoribbons (ZGNRs).²⁷⁻²⁹ Our recent study on conjugated donor-acceptor (D-A) polymers indicate that an end localized spin topology facilitates a high-spin ground-state with a significant population of triplet states at room temperature, 20 which can be synthetic targets for room temperature magnetic materials in the pristine form. This indicates that not only the ground-state of OSCs but also their spin-ordering can be manipulated by the spin distribution along the material's backbone. Therefore, controlling the spin topology and spin alignment in the alternating D-A polymers is in the best interest of spintronics and magnetic devices.

Fig. 1 (a-c) Prototypical examples of molecules with non-Aufbau orbital ordering in different charged states. (d) Molecular and resonance structures of the high-spin state (S = 1) polymers with a variable spin distribution, where modulation of aromaticity in the auxiliary ring (light purple color) tunes the spin topology and orbital ordering varying from Aufbau to non-Aufbau studied in this work.

The ordering of electrons in MOs follows the widely accepted Aufbau principle, which states that the lowest energy orbitals are filled first, and the singly occupied MOs (SOMOs) should be higher in energy than the highest occupied MOs (HOMOs). However, there are exceptions (Fig. 1a-c) to this widely accepted principle, where implications of the non-Aufbau principle are realized due to the unusual SOMO-HOMO energy level inversion. 30-32 Materials with a non-Aufbau orbital ordering are technologically relevant in both conducting and magnetic-based applications.³³ Interestingly, the SOMO-HOMO energy level inversion is only reported in radical species, 26,30-39 and recently has been observed in cyclic carbenes. 40 Oneelectron oxidation of these species produces a high-spin triplet ground-state. However, the intrinsic non-Aufbau orbital ordering is not reported for open-shell high-spin ground-state polymers in the neutral state.

We report D-A conjugated polymers comprised of a donor unit, cyclopentadiselenophene (CPDS), and a different non(semi)-metallic element (C, Si, N, and Se) substituted benzobis[1,2-c;4,5-c']bis[1,2,5]thiadiazole (BBT) CBBT, SiBBT, NBBT, and SeBBT, respectively (Fig. 1d). The ease of tunability of the molecular topology of D-A polymers provides an opportunity for tailoring their properties and facilitates a broad range of applicability. 4,23,41-45 We employed the atomistic engineering technique by replacing the sulfur atom in one of the thiadiazole units of the BBT acceptor by C, Si, N, and Se, respectively, which enabled tuning their orbital topologies. Significant amounts of studies have been conducted based on the idea of atomistic engineering, which is almost exclusively focused on tuning the molecular band gap so as to have red-shifted absorption in the solar spectrum. 46-58 However, a thorough study delineating the effect of heteroatoms on the spin topology of high-spin ground-state molecules is not available in the literature.

2 Computational details

Geometry optimizations are performed with the Gaussian 16 software package⁵⁹ without any symmetry constraints. Molecular geometries for the electronic singlet (S = 0) and triplet (S = 1)states of the model oligomers (N = 1 to 8) are optimized using the hybrid density functional B3LYP. 60,61 For Si and Se atoms, the LANL2DZdp basis set is used along with associated effective core potentials^{62,63} and the 6-31G(d,p)⁶⁴ basis set is used for other atoms. All parameters for geometry optimizations are set to default. UltraFine grids are used for numerical integration (see Table S1 for comparison with other grids, ESI†). As we can see, increasing the number of grid points does not affect the electronic properties. For larger oligomers, geometries are considered optimized once the forces on all atoms are converged to zero.65 Unless otherwise specified, analyses are performed with the (U)B3LYP level of theory. Full computational details can be found in ref. 9 and 20.

We have performed a dihedral scan along the connecting bond of the donor unit and the acceptor unit of a monomer to

identify the lowest energy conformer (see Fig. S1, ESI†). Therefore, all polymers considered in the present work are arranged according to their minimum energy conformations. Our previous work shows that the minimum energy configuration connects the olefin unit to the donor in an alternating arrangement. 20 As a result, we arranged the thiadiazole units in an alternating manner. We have also performed calculations on a dimer by arranging all the thiadiazole units on the same side and compared the stability of these two configurations with the singlet-triplet energy gap (see Table S2, ESI†). As we can see, arranging the thiadiazole units in an alternating manner results in a more stable configuration than arranging all the thiadiazole units in the same direction, except for CPDS-SeBBT, where both configurations are equally likely. However, as we are taking the difference between the energies of the singlet and triplet states, the differences in the singlet-triplet energy gap ($\Delta E_{\rm ST}$) are minimal.

A broken-symmetry (BS)⁶⁶ wave function is used to optimize and characterize the open-shell singlet state. As spin contamination is a potential issue, we report the expectation value of the total spin-squared operator in the ESI† (Table S1) for Hartree-Fock (HF) and B3LYP methods. Compared to HF, B3LYP provides the expectation value close to 1, which is the expected value for the broken symmetry approach that admixes singlet and triplet states.1 The triplet state is optimized with an unrestricted wave function. The location of the unpaired spins is predicted with the NBO7 program package⁶⁷. The isotropic nucleus independent chemical shift (NICS_{iso}(1))⁶⁸ is computed with the gauge-independent atomic orbital (GIAO)⁶⁹ at 1 Å above the ring plane, where a large negative NICS_{iso}(1) is an indication of an aromatic structure. The anisotropy of the induced current density (ACID) method⁷⁰ at the CSGT-UB3LYP/6-31G(d,p) level of theory⁷¹ is used to generate the ring current density and rendering is performed with a locally developed code. The 2D-ICSS (2D-isochemical shielding surface) maps are generated by the method developed by Klod et al.72 The harmonic oscillator model of aromaticity (HOMA)73 is calculated with

HOMA =
$$1 - \frac{98.89}{n} \sum_{i=1}^{n} (R_i - 1.397)^2$$
 (1)

where n is the number of bonds considered in a particular ring and R_i is the optimized bond length at the equilibrium geometry. HOMA = 1 indicates an aromatic structure. 73,74 The optimally tuned range-separated hybrid functional (OT-RSH) calculations are performed with the LC-ωHPBE functional⁷⁵, where the rangeseparated parameter, ω , is determined by the ionization potential (IP) scheme.⁷⁶ Molecular orbital diagrams and spin density plots are generated with VMD.77

3 Results and discussion

3.1 Selection of donor and acceptor units and different heteroatoms

We have selected C-bridged cyclopentadiselenophene (CPDS) as a donor unit, which can increase the π -conjugation, elevate the highest occupied molecular orbital (HOMO), induce a more planar molecular backbone, and can increase the quinoidal character by decreasing the orbital overlap with the π -system due to a large C-Se bond in the donor unit.9,49 The BBT acceptor, on the other hand, has a large electron affinity and a lower lowest unoccupied MO (LUMO), which can reduce the HOMO-LUMO energy gap.³ A smaller energy gap facilitates the admixing of the frontier MOs (FMOs) into the ground-state, generating open-shell character. 3,9,78-80 The selection of heteroatoms from different groups facilitates assessing the effect of various elements in the periodic table, whereas previous studies mainly focused on atomistic substitution based on one particular group elements. 46,81 Substitution of different heteroatoms into the thiadiazole unit of the BBT acceptor changes the hybridization of the particular atoms and changes the aromatic character of the thiadiazole unit. The C and Si atoms are sp³ hybridized, which reduces the aromatic character of the thiadiazole unit. On the other hand, the N atom is sp² hybridized, and substitution of the N atom increases the aromatic character of the thiadiazole unit. Therefore, changing the hybridization of the heteroatoms modulates the bond length alternation (BLA) in the thiadiazole units, hence significantly changing the local aromatic/quinoidal character46,48,49 of the BBT acceptor; therefore, a distinct change in the electronic properties and spin topologies is observed. A highly quinoidal molecular backbone can increase the open-shell character and reduce the singlet-triplet energy gap (ΔE_{ST}) . 9,48 Furthermore, the heteroatom (C, Si, and N) inclusion facilitates the addition of more solubilizing -CH₃ groups, which not only will increase the solubility in conventional solvents but also will kinetically block the reactive sites, increasing the stability of the polymers.4,19,23

3.2 Effect of different heteroatoms on orbital ordering

We have extensively analysed the MOs along with their energies to gain insights into the nature of SOMO-HOMO energy level inversion in these different polymers and establish a design paradigm. This can facilitate designing novel materials with intriguing orbital ordering in the neutral state. Interestingly, the orbital ordering is exclusively modulated by the different atomistic substitutions. For example, the C, Si, and Se atom substituted polymers show a non-Aufbau orbital ordering. However, the orbitals are ordered according to the increased energy in the N substituted CPDS-NBBT polymer (see Fig. S2-S21, ESI†), following the Aufbau principle.

In the case of a smaller repeat unit (N = 2) for the C substituted polymer (Fig. S2, ESI \dagger), spin-orbital 235 α (α -SOMO) is higher in energy and localized at one end of the π -conjugated backbone. Therefore, it constitutes one of the unpaired electrons in the diradical polymer. The β spins are mostly delocalized along the polymer backbone. However, the frontier spin-orbital 235β (β-SOMO) has the same spatial distribution and energy as the 234α (α-SOMO-1) spin-orbital, making these two orbitals resemble as a closed-shell configuration (i.e., a HOMO). Therefore, the 234β (β-SOMO-1) spin-orbital acts as another unpaired electron, which indicates that the non-Aufbau orbital ordering is observed even in the smallest repeat unit of the C substituted polymer.

Looking at the spatial orientations and energies of the MOs, there are four unpaired electrons in the CPDS-CBBT dimer (Fig. S2, ESI†). However, there is no polyradical character observed in the studied polymers (Table S3, ESI†), which has also been reported for other BBT-based materials. 8,78 This is probably due to the fact that the unpaired electrons which are deeper in energy do not contribute to the open-shell character, limiting the open-shell character to diradicals (see Table S3, ESI†). A similar phenomenon in orbital orientation is observed for the Si substituted polymer as well (Fig. S6, ESI \dagger). However, in the case of smaller units (N = 2) of N and Se substituted polymers, normal Aufbau orbital ordering is observed (Fig. S10 and S14, ESI†).

Increasing the oligomer chain length (N = 4-8) downshifts the unpaired β spin for C, Si, and Se substituted polymers. For example, in the case of the CPDS-SiBBT tetramer (N = 4), spin orbital 466β (β-SOMO-3) is out of phase with the frontier α -SOMO (Fig. S7, ESI[†]). However, for the octamer (N = 8), β-SOMO-6 (931β) is similar to the α-SOMO with respect to the orbital pattern (Fig. 2). Due to the large Coulomb repulsion in placing an unpaired electron into the spatially delocalized

SOMOs, the β-spin is pushed downward in energy, providing a non-Aufbau orbital orientation.¹⁷ We have also analysed the orbital orientations and energies of the CPDS-SiBBT tetramer (N = 4) with BLYP⁶⁰, CAM-B3LYP,⁸² ω B97X-D,⁸³ and OT-RSH (LC- ω HPBE(ω = 0.90)) methods. These functionals also provide a non-Aufbau orbital configuration (Fig. S18-S21, ESI†), which indicates that the non-Aufbau orbital orientation is an intrinsic property of the CPDS-SiBBT polymer. On the other hand, the α-SOMO and β-SOMO of the CPDS-NBBT octamer have different spatial orientations and energies, which indicates that these two spin-orbitals constitute the frontier molecular orbitals (Fig. S13, ESI†). As a result, the orbital orientation follows the normal Aufbau principle according to the increase in energy. This indicates that the orbital arrangement is modulated by different atomistic substitutions, which is observed even in the smallest repeat units. Interestingly, when an asymmetric arrangement is considered for the polymers, such as end-capping with donor or acceptor units, we observed two different scenarios. When the CPDS-SiBBT heptamer (N = 7) is end-capped with acceptor units, the two spin-orbital α -SOMO-7 (864 α) and β -SOMO-13 (861 β)

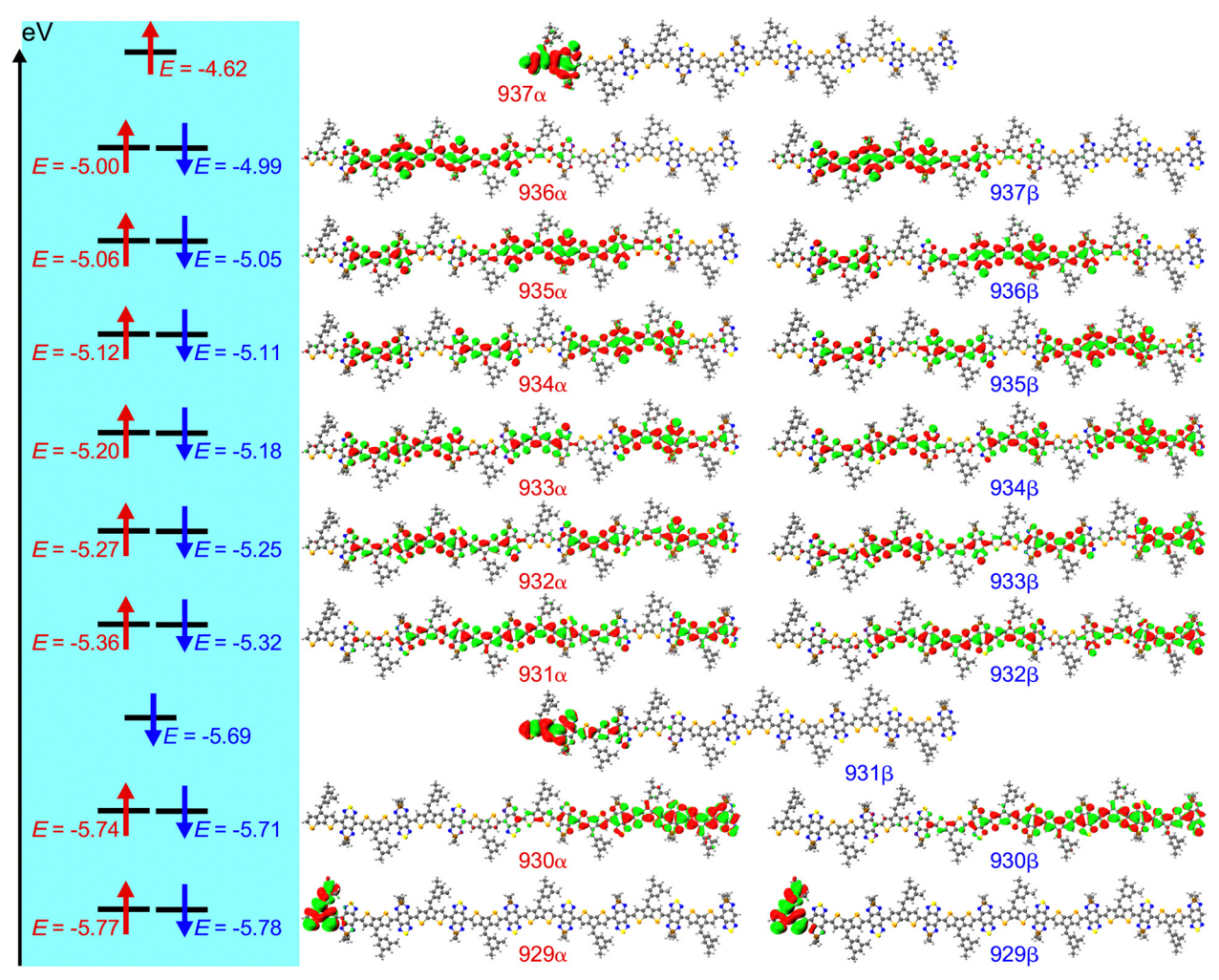


Fig. 2 Molecular orbitals (MOs) and their energies at the singlet (S = 0) state for the CPDS-SiBBT octamer (N = 8). The green and red surfaces represent positive and negative contributions of the MOs at an isovalue = 0.01 a.u.

are lower in energy than the HOMOs (Fig. S22, ESI†). This indicates that the CPDS-SiBBT polymer when end-capped with the BBT acceptor shows non-Aufbau orbital ordering. However, when the polymer is end-capped with donor units, the frontier α-SOMO (886α) and β-SOMO (886β) are arranged according to the Aufbau principle (Fig. S23, ESI†). Therefore, the Aufbau orbital ordering and non-Aufbau orbital ordering are also being modulated with different end groups in the CPDS-SiBBT polymer.

The driving force for this unique orbital orientation originates from the different atoms substituted into the thiadiazole unit of the BBT acceptor since these heteroatom substitutions modulate the local aromatic character of the thiadiazole units, which alters the aromatic/quinoidal character along the polymer's backbone. We have analysed the bond length of the substituted BBT acceptor unit and performed NICS_{iso}(1) and 2D-ICSS calculations to assess the aromatic character. Bond length analysis indicates that substitution of different heteroatoms significantly alters the bond length of the thiadiazole unit. The N-S bond of the unsubstituted thiadiazole unit in the singlet state (S = 0) is ≈ 1.65 Å, whereas the N-X (X = C, Si, N, and Se) bond varies as 1.47-1.48, 1.77-1.78, 1.32-1.33, and 1.81-1.82 Å in the CPDS-CBBT, CPDS-SiBBT, CPDS-NBBT, and CPDS-SeBBT polymers (N = 8), respectively (see Tables S4–S7, ESI†). The largest N-X bond is observed in the Se substituted thiadiazole unit due to the larger atomic size of the Se atom and the smallest N-X bond is predicted in the CPDS-NBBT polymer. As a result, the Se substituted thiadiazole unit should show the least aromatic character and the N substituted thiadiazole unit provides the strongest aromaticity. 48 The C-N (L1 and L4 in Tables S4-S7, ESI†) bond of the unsubstituted thiadiazole unit is \approx 1.33 Å, which is close to a double-bond. In the case of the C and Si substituted polymers, the C-N (L5 and L8 in Tables S4-S5, ESI†) bond is more reduced (≈ 1.30 Å), increasing the doublebond, and hence the quinoidal character of the substituted thiadiazole unit. The largest C-N (L5 and L8 in Table S6, ESI†) bond ($\approx 1.35 \text{ Å}$) is observed for the N substituted polymer, which is also close to the N-N bond (L6 and L7 in Table S6, ESI†). Therefore, the N substitution equalizes the bond length in the thiadiazole unit of the CPDS-NBBT polymer, increasing the aromatic character of the polymer backbone.

This has been reflected in the observed NICS_{iso}(1) values as well (see Tables S8-S23, ESI†). The largest (more negative) calculated NICS_{iso}(1) value is observed for the N substituted thiadiazole unit (ring 8D) (\approx -12.50 ppm), whereas the smallest (less negative) NICS_{iso}(1) value is observed for the CPDS-SiBBT polymer (ring 8F) (\approx -2.90 ppm) (Tables S15 and S19, ESI†). Although the N substituted thiadiazole unit provides a large aromatic character due to a smaller N-N bond, the largest N-Se bond containing thiadiazole unit (8F) does not show the least aromatic character (NICS_{iso}(1) \approx -9.88 ppm) (Table S23, ESI†). In the open-shell form, the hypervalent Se atom goes from high-energy N=Se=N to N-Se-N configuration by recovering aromatic stabilization energy in the thiadiazole unit, which facilitates achieving a high open-shell diradical character in the CPDS-SeBBT polymer. 20 The 2D-ICSS maps indicate that both the thiadiazole units of the CPDS-SeBBT polymer are magnetically shielded (negative 2D-ICSS: aromatic) (Fig. 3). On the other hand, the thiadiazole unit with the substituted heteroatoms in the CPDS-CBBT and CPDS-SiBBT polymers is magnetically de-shielded (less negative 2D-ICSS: quinoidal) and the unsubstituted thiadiazole unit is magnetically shielded

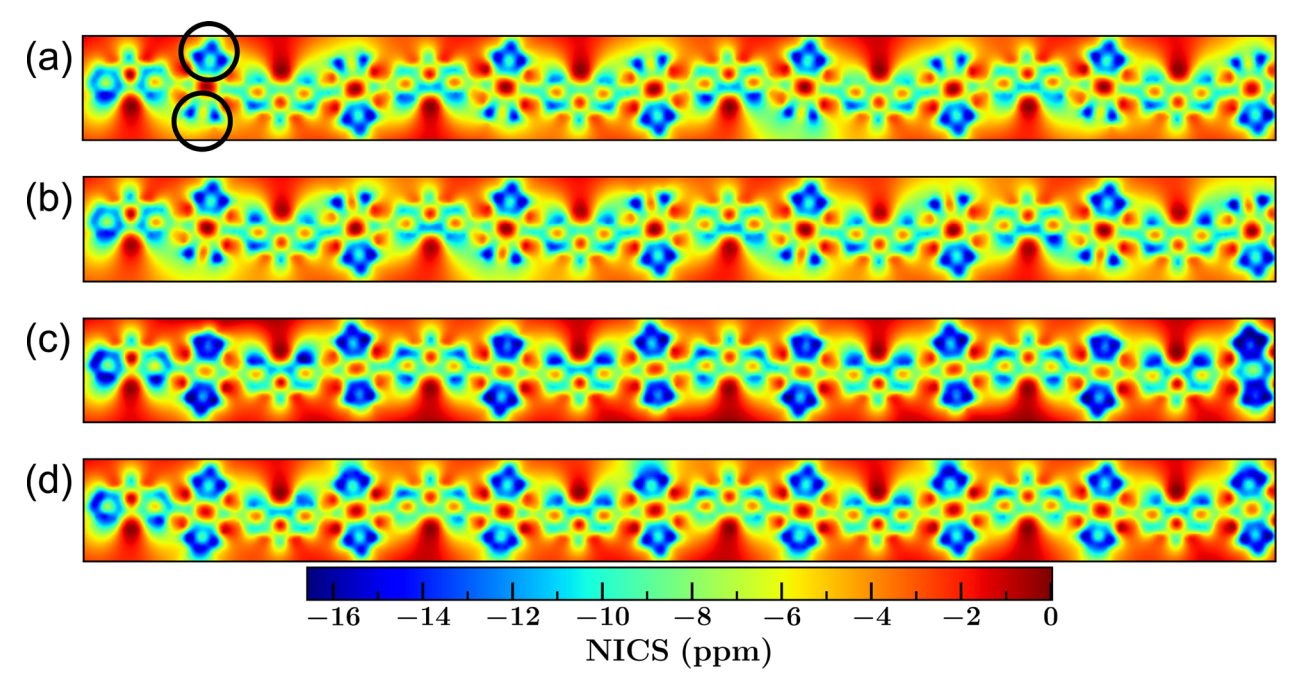


Fig. 3 Calculated 2D-ICSS maps for the (a) CPDS-CBBT, (b) CPDS-SiBBT, (c) CPDS-NBBT, and (d) CPDS-SeBBT polymers (N = 8) in the triplet (S = 1) state. The change in the aromatic character of the substituted and unsubstituted thiadiazole units for CPDS-CBBT is highlighted with black open circles.

(Fig. 3). Therefore, although the Se substituted polymer has the largest N-Se bond, the bond polarization is largest in the case of the Si substituted polymer due to a large difference in the element's electronegativity. 48 Also, due to a change in the element's hybridization, the aromatic/quinoidal character changes in the thiadiazole units of the BBT acceptor, which modulates the orbital ordering of the studied polymers.

3.3 Effect of different heteroatoms on the spin density distribution

Modulation of the spin density distribution controls the ground-state electronic and magnetic properties.^{5,20} We have analysed the spin density distribution along with the spin values as a function of oligomer chain length (see Fig. S24-S48, ESI†). As can be seen from Fig. 4, except for the CPDS-NBBT polymer, all the polymers significantly localize the spin densities at the two opposite ends, as observed in the BBT-based polymers.²⁰ The most spin localization is achieved in the CPDS-SiBBT polymer compared to the other polymers, where spin localization is visible from the dimer (N = 2) (see Fig. S46, ESI†). Increasing the oligomer chain length further localizes the unpaired electrons at the two opposite ends of the C, Si, and Se substituted polymers compared to the N substituted polymer due to the delocalized nature of the sp² hybridized N atom (Fig. 4 and Fig. S46-S48, ESI†), which indicates that the atomistic substitution modulates the spin density in the studied polymers.

By analysing the MOs and spin density distribution, we observe a disparity between the SOMOs and spin density distribution for CPDS-CBBT, CPDS-SiBBT, and CPDS-SeBBT polymers, which have a non-Aufbau orbital ordering. For example, the SOMOs of the C, Si, and Se substituted polymers are located on the same side of the polymers, whereas the spin density is localized at the two opposite ends (Fig. S24-S45, ESI†). Therefore, the SOMOs have a very small contribution in the total spin density for the C, Si, and Se polymers compared

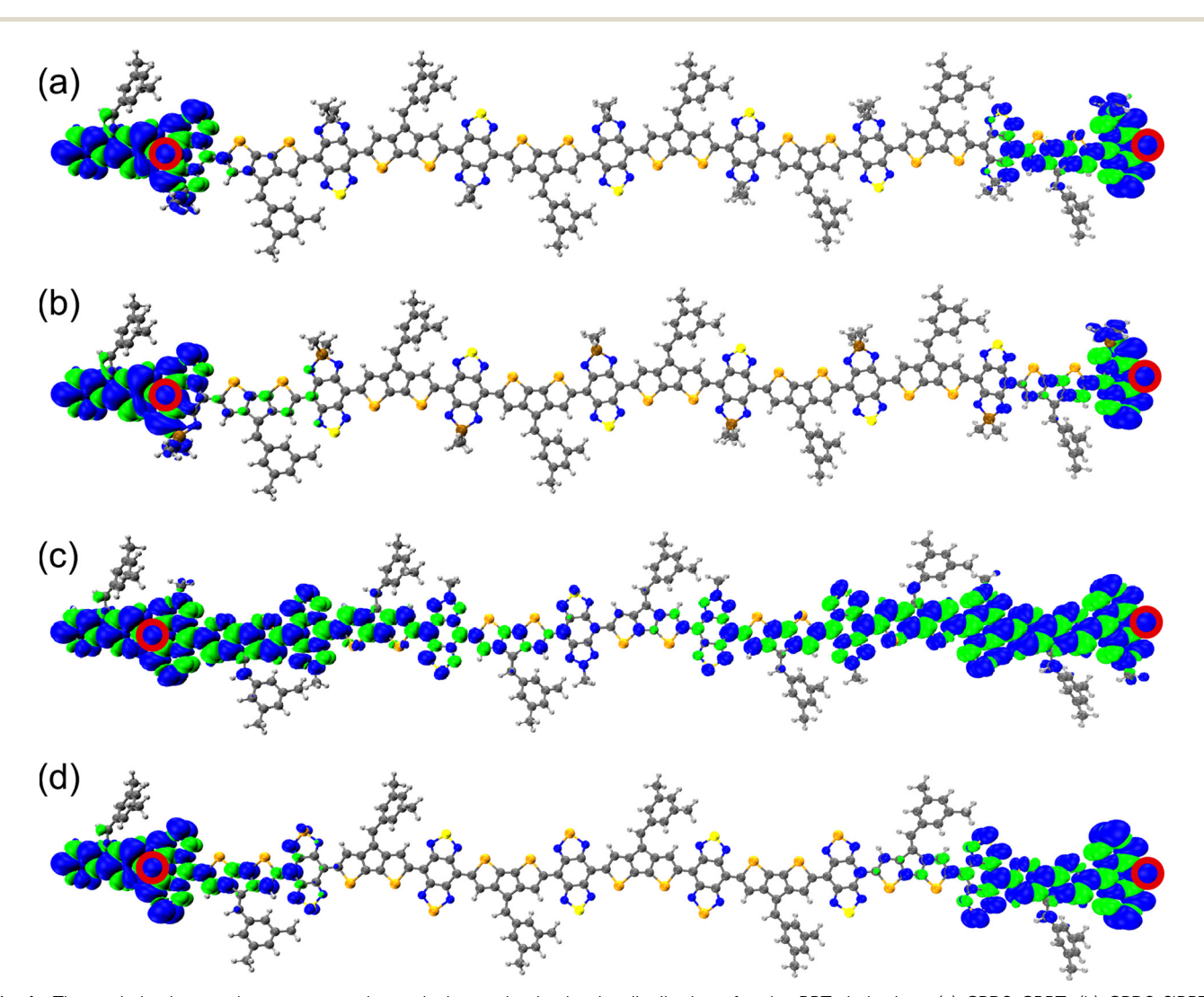


Fig. 4 The optimized ground-state geometries and observed spin density distributions for the BBT-derivatives, (a) CPDS-CBBT, (b) CPDS-SiBBT, (c) CPDS-NBBT, and (d) CPDS-SeBBT (N = 8) polymers in their triplet (S = 1) state. The blue and green surfaces represent positive and negative contributions of the spin density at an isovalue = 0.0002 a.u. The most probable locations of the unpaired electrons are highlighted with open circles.

to the N substituted polymer. Accumulation of the fractional contributions from the MOs probably leads to an end localized spin density distribution on the C, Si, and Se substituted polymers.

Variation of the aromatic character along the polymer backbone facilitates spin separation in the BBT-based materials.²⁰ To rationalize the different spin density distributions, we have analysed the aromatic/quinoidal character with bond lengths along the polymer's backbone. The calculated bond lengths along the conjugated path (Fig. 5 and Tables S24-S27, ESI†) in the benzenoid ring of the BBT core vary within 1.413-1.493, 1.418-1.546, 1.398-1.448, and 1.409-1.460 Å in the CPDS-CBBT, CPDS-SiBBT, CPDS-NBBT, and CPDS-SeBBT polymers, respectively. This indicates that the bond length alternation (BLA) is largest in the CPDS-SiBBT polymer, whereas BLA is significantly reduced in the N substituted polymer. Therefore, the CPDS-SiBBT polymer has the most quinoidal backbone compared to

the other polymers. As a result, the Si substituted polymer has the most localized spin density distribution and spins are significantly polarized compared to the other polymers. On the other hand, the CPDS-NBBT polymer shows almost delocalized spin distribution along the whole backbone. The calculated spin values are largest at the two opposite ends of the polymers, and the singlet (S = 0) and triplet (S = 1) states have the same positive values (Fig. S49 and S50, ESI†). Interestingly, the N atom adjacent to the C, Si, and Se heteroatoms shows a very high spin value, whereas the same N atom has essentially no spin in the CPDS-NBBT polymer. This also indicates that the bond polarization is significant in the CPDS-CBBT, CPDS-SiBBT, and CPDS-SeBBT polymers than in the CPDS-NBBT polymer. These highly spin-polarized polymers can be used as a building block for spintronic devices.33

Increasing the oligomer chain length increases the quinoidal character at the core of the polymers, whereas both ends become

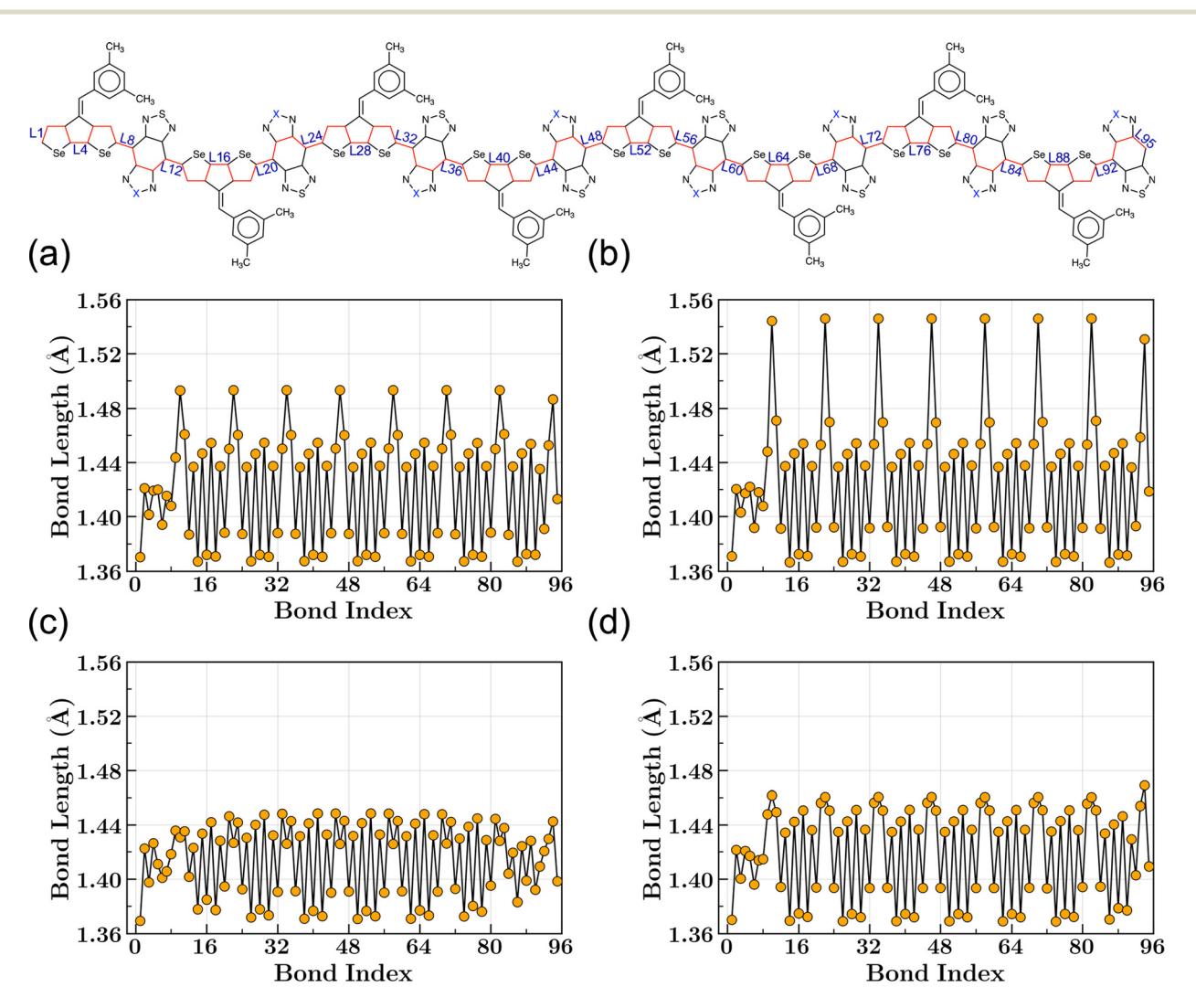


Fig. 5 The calculated bond lengths of the (a) CPDS-CBBT (X = C), (b) CPDS-SiBBT (X = Si), (c) CPDS-NBBT (X = N), and (d) CPDS-SeBBT (X = Se) polymers (N = 8) along the highlighted π -conjugated path. Bond lengths computed at the UB3LYP/6-31G(d,p) level of theory and basis set are provided for the triplet (S = 1) state. Different atomistic substitutions change the BLA along the conjugation backbone, changing the electronic properties and spin distribution

Paper

more aromatic (see Tables S8-S23, ESI†). For example, ring 1A of the CPDS-CBBT octamer has a NICS_{iso}(1) value of \approx -7.06 ppm, whereas ring 4A shows a significantly reduced aromatic character (≈ -3.60 ppm) (see Table S11, ESI†). The benzenoid ring (4E) at the polymer core indicates a very small (less negative) NICS_{iso}(1) value (≈ -0.25 ppm) than the benzenoid ring (8E) at the chain end (\approx -0.96 ppm). Similar phenomena are observed in the CPDS-SiBBT, CPDS-NBBT, and CPDS-SeBBT polymers as well (see Fig. S51, ESI†). The 2D-ICSS maps also show increased magnetic shielding at both end units, indicating an increased aromatic character (Fig. 3). Therefore, the spins are separated from the large quinoidal core to the more stable aromatic ends, localizing spins to the two opposite ends of the polymers (Fig. 4 and Fig. S46-S48, ESI†).

3.4 Effect of different heteroatoms on the singlet-triplet energy gap (ΔE_{ST})

The characteristic features of the open-shell materials are best described by the energy difference between the ground-state and the lowest excited-state, and open-shell character. All the calculated electronic properties for the polymers are provided in Table 1 and Table S3 (ESI†). The trend in the calculated singlet-triplet energy gap ($\Delta E_{\rm ST}$) provides insights into the role of addition of different heteroatoms and the oligomer chain length. The observed $\Delta E_{\rm ST}$ and open-shell character are entirely dependent on the different heteroatoms substituted into the thiadiazole unit of the BBT acceptor.

The effect of substituting different heteroatoms on the acceptor unit is visible at a smaller oligomer unit from the calculated $\Delta E_{\rm ST}$ and diradical character (y₀). At the monomer unit (N = 1), ΔE_{ST} for the Se substituted polymer (CPDS-SeBBT) is 0.114 eV smaller (Table S3, ESI†) than that of our previously reported CPDS-BBT polymer.9 This indicates that, in the same

Table 1 Computed electronic properties at the (U)B3LYP/6-31G(d,p) level of theory and basis set for the CPDS-CBBT, CPDS-SiBBT, CPDS-NBBT, and CPDS-SeBBT polymers as a function of chain length (N). The singlettriplet energy gap ($\Delta E_{ST} = E_S - E_T$), population (P_T) of the triplet (S = 1) state at room temperature, energies of the highest occupied MO (HOMO) and the lowest unoccupied MO (LUMO), energetic difference between the FMOs (E_g), and diradical character index (y_0) of the polymers. Energy values are in eV, and y_0 is a dimensionless quantity

Polymer	N	$\Delta E_{ m ST}$	P_{T}	номо	LUMO	$E_{ m g}$	yo
CPDS-CBBT	2	-5.33×10^{-4}	74.63	-4.64	-3.37	1.27	0.974
	4	$+2.72 \times 10^{-7}$	75.00	-4.58	-3.41	1.17	1.000
	6	0.00×10^{-0}	75.00	-4.57	-3.42	1.15	1.000
	8	0.00×10^{-0}	75.00	-4.57	-3.43	1.14	1.000
CPDS-SiBBT	2	$+3.90 \times 10^{-4}$	75.27	-4.69	-3.49	1.20	0.999
	4	0.00×10^{-0}	75.00	-4.64	-3.53	1.11	1.000
	6	0.00×10^{-0}	75.00	-4.63	-3.54	1.08	1.000
	8	0.00×10^{-0}	75.00	-4.62	-3.55	1.07	1.000
CPDS-NBBT	2	-2.13×10^{-1}	0.12	-4.35	-3.11	1.24	0.193
	4	-2.78×10^{-2}	51.93	-4.15	-3.19	0.96	0.838
	6	-4.01×10^{-3}	72.14	-4.09	-3.22	0.87	0.977
	8	-5.82×10^{-4}	74.60	-4.07	-3.23	0.85	0.997
CPDS-SeBBT	2	-1.86×10^{-2}	60.27	-4.60	-3.45	1.16	0.832
	4	-5.88×10^{-5}	74.96	-4.49	-3.48	1.00	0.995
	6	0.00×10^{-0}	75.00	-4.46	-3.49	0.97	1.000
	8	0.00×10^{-0}	75.00	-4.45	-3.50	0.95	1.000

group of the periodic table, increasing the atomic size and a reduction in electronegativity should reduce the singlet-triplet energy gap. Also, a similar phenomenon is observed for the C and Si substituted polymers, CPDS-CBBT and CPDS-SiBBT, receptively, where a larger atom with reduced electronegativity reduces $\Delta E_{\rm ST}$ and increases the open-shell diradical character. However, this directly contradicts the recent findings from Wu et al., where it is reported that increasing the heteroatomic size increases $\Delta E_{
m ST}$ and reduces the diradical character. 81 On the other hand, the N substituted polymer CPDS-NBBT shows a closed-shell $(y_0 = 0)$ structure with the largest calculated ΔE_{ST} (0.657 eV at N=1) among the studied polymers (see Table S3, ESI†). This indicates that atomistic substitution can modulate the electronic properties of the studied polymers.

Increasing the oligomer length reduces the ΔE_{ST} gap, as observed from previous studies. 9,19,20 Except the CPDS-NBBT polymer, the CPDS-CBBT, CPDS-SiBBT, and CPDS-SeBBT polymers show a large diradical character even at the monomer (N = 1) unit (see Table S3, ESI†), which indicates that the openshell form is more stable in energy than the closed-shell configuration. This is visible from the energy diagram (Fig. S52, ESI†), where the closed-shell state of the CPDS-CBBT dimer (N = 2) is 15.4 kcal mol⁻¹ above the reference singlet open-shell state. On comparing the energy difference between the open-shell and closed-shell state in the smaller repeat unit, the largest value is obtained for the CPDS-SiBBT dimer (17.3 kcal mol⁻¹), indicating a larger diradical character in a smaller repeat unit. However, the closed-shell configuration of the CPDS-NBBT dimer is close to a degenerate state with its open-shell configuration, showing a very small diradical character for this polymer in the smaller repeat unit. As the number of repeat units is increased, a rapid decrease in the ΔE_{ST} gap is observed for the C, Si, and Se substituted polymers compared to the N substituted polymer. The Se substituted polymer shows a degenerate ΔE_{ST} gap at N = 6repeat units, whereas the N substituted polymer has a large $\Delta E_{\rm ST}$ gap even at N = 8 (Table 1 and Table S3, ESI†). Extrapolation of the computed $\Delta E_{\rm ST}$ gap with the number of repeat units indicates that an inflection point is achieved at N = 9 (Fig. S53, ESI†), which indicates that CPDS-NBBT has a high-spin triplet (S = 1) groundstate at a larger repeat unit. In the case of the C substituted polymer CPDS-CBBT, a triplet (S = 1) ground-state is observed at N = 3, whereas the dimer (N = 2) of CPDS-SiBBT shows a triplet ground-state (Table 1 and Table S3, ESI†). However, the larger oligomers of CPDS-CBBT, CPDS-SiBBT, and CPDS-SeBBT show a degenerate energy state between the singlet and triplet states. The thermal population of the triplet state increases as the oligomer units are increased. The CPDS-NBBT polymer has no triplet state population for the monomer (N = 1) unit; however, a significant population (55.99%) is observed for CPDS-SiBBT at room temperature (Table S3, ESI†). The dimer of the CPDS-SiBBT polymer surpasses the threshold population of a degenerate state (75.00%), providing the largest value (75.27%) among the studied

A stronger π-conjugation can increase the electronic coherence along the polymer backbone.9 All the polymers possess small dihedral angles between the adjacent donor and acceptor

units, which indicates a strong π -conjugation throughout the π framework. The connecting bonds between the adjacent donor and acceptor units in the triplet state (S = 1) vary within 1.387-1.408, 1.391-1.408, 1.390-1.420, and 1.393-1.415 Å for the CPDS-CBBT, CPDS-SiBBT, CPDS-NBBT, and CPDS-SeBBT polymers, respectively (Fig. 5 and Tables S24-S27, ESI†). This indicates that the C and Si substituted polymers have a larger π -conjugation than the N and Se substituted polymers, with the least conjugation being observed for the N substituted CPDS-NBBT polymer. Therefore, the π -conjugation of the CPDS-CBBT, CPDS-SiBBT, CPDS-NBBT, and CPDS-SeBBT polymers is modulated with different atomistic substitutions as well. The addition of more repeat units increases the distance between the unpaired electrons of the polymers (Fig. S54, ESI†), which reduces the Coulomb repulsion. As a result, the triplet state (S = 1) becomes lower in energy than the singlet (S = 0)state at a larger repeat unit, generating a high-spin triplet ground-state.

3.5 Effect of different heteroatoms on the open-shell character

The presence of unpaired electrons in the open-shell OSCs can be quantitatively described by the radical indices, y_i (i = 0-1). y_0 and y_1 represent diradical and tetraradical character, respectively, where the indices range from $0 \le y_i \le 1$. For example, $y_0 = 0$ indicates a closed-shell structure and $y_0 = 1$ indicates a pure open-shell diradical character. 84-86 The calculated diradical character is provided in Table 1 and in the ESI† (see Table S3) as a function of chain length. It is clear from the calculated diradical character that increasing the oligomer chain length increases y_0 , as observed in other studies. ^{19,20} Although the analysis of MOs indicates the presence of more than two unpaired electrons in these polymers, the calculated tetraradical character is very low ($y_1 < 0.10$).

Different atomistic substitutions provide variable open-shell diradical character, which is evident in the smaller repeat units. For example, the Si substituted polymer CPDS-SiBBT shows a very high open-shell character ($y_0 = 0.787$) even at the monomer (N = 1) unit. However, the N substituted polymer CPDS-NBBT shows a closed-shell configuration ($y_0 = 0.0$) (see Table S3, ESI†). The dimer of CPDS-NBBT shows a very small diradical character ($y_0 = 0.193$), which indicates that the open-shell and closed-shell configurations are degenerate in energy (Fig. S52, ESI†). On the other hand, the Se substituted polymer shows a moderate open-shell character for the smaller repeat units, and the open-shell character quickly approaches the bond dissociation limit $(y_0 = 1.0)$ for C and Si substituted polymers (Table 1 and Table S3, Fig. S55, ESI†). This indicates that the preference for a high-spin triplet (S = 1) ground-state is largest in the Si and C substituted polymers, and least in the CPDS-NBBT polymer. This is readily visible from the calculated $\Delta E_{\rm ST}$ gap as well, where the $\Delta E_{\rm ST}$ gap is very high even at the octamer (N = 8) of the N substituted polymer; however, the CPDS-CBBT, CPDS-SiBBT, and CPDS-SeBBT polymers show a degenerate $\Delta E_{\rm ST}$ gap at the larger repeat units with a significant population of the triplet state at room temperature (see Table 1 and Table S3,

ESI†). Also, the addition of more repeat units gradually reduces the HOMO-LUMO energy gap (Table 1 and Table S3, Fig. S56, ESI†). A small energy gap facilitates admixing of the FMOs into the ground-state, developing open-shell diradical character.

The thiadiazole units of the BBT acceptor recover aromatic stabilization energy in the open-shell configuration, as observed in the previous studies. 20, 78 However, the substitution of different heteroatoms significantly alters the local aromatic character of the thiadiazole units. For example, the calculated $NICS_{iso}(1)$ value of the CPDS-BBT $(N = 8)^{20}$ unsubstituted thiadiazole unit in the singlet state (S = 0) is ≈ -9.8 ppm, which indicates a large local aromatic character compared to that of the six-membered benzenoid ring (≈ -1.1 ppm). The corresponding NICS_{iso}(1) value changes according to the substituted heteroatoms: the smallest value (less negative) is observed in the Si substituted CPDS-SiBBT polymer (N = 8) $(\approx -2.82 \text{ ppm for the 4F unit})$ (Table S15, ESI†) and the largest value (more negative) is observed in the N substituted CPDS-NBBT polymer (N = 8) (\approx -11.32 ppm for the 4D unit) (Table S19, ESI†). This indicates that insertion of the Si atom reduces the aromatic character and increases the quinoidal character in the thiadiazole unit, which increases the diradical character. However, the N substitution imparts more aromatic character in the CPDS-NBBT polymer backbone, reducing the diradical character. The C and Se substituted polymers show similar reduced aromatic character in the thiadiazole units (-5.45) and -9.31 ppm, respectively); however, the observed NICS_{iso}(1) is significantly larger (more negative) than that of the Si substituted polymer.

Substitution of different heteroatoms affects the aromatic/ quinoidal character of the polymer's backbone, which consequently modulates the open-shell character and orbital topology. Analysis of BLA along the conjugated backbone indicates that the dimer (N = 2) shows a very small BLA compared to the larger repeat unit (Fig. S57-S72, ESI†). Different atomistic substitutions provide a different BLA: the largest BLA is observed for the Si substituted polymer, whereas the BLA is significantly reduced for the N substituted polymer. This indicates that CPDS-SiBBT possesses the largest open-shell diradical character compared to the other polymers, which is observed in the calculated diradical index (Table 1 and Table S3, ESI†). In the case of CPDS-SiBBT, the calculated NICS_{iso}(1) value for the benzenoid rings is positive (Tables S12-S15 and Fig. S51, ESI†), which indicates that the backbone of the CPDS-SiBBT polymer is more quinoidal than that of the other polymers, which is also reflected in the observed BLA value. The calculated HOMA values show that the CPDS-SiBBT polymer has the smallest HOMA values (less aromatic), and a larger value (more aromatic) is observed for the CPDS-NBBT polymer (Fig. S73, ESI†), which is in line with the NICS_{iso}(1) and BLA calculations. The ACID plots show that the thiadiazole units of the CPDS-NBBT and CPDS-SeBBT polymers have two clear clockwise (diatropic) ring currents, which indicates large local aromaticity (Fig. 6). On the other hand, the heteroatom substituted thiadiazole units of the CPDS-CBBT and CPDS-SiBBT polymers show counter-clockwise (paratropic) ring currents, an indication of reduced aromaticity. Although the cores of (d)

Paper

(a) (b) (c)

Fig. 6 ACID plots for the (a) CPDS-CBBT, (b) CPDS-SiBBT, (c) CPDS-NBBT, and (d) CPDS-SeBBT polymers (N = 8) in the triplet (S = 1) state. The clockwise (diatropic: aromatic) and counterclockwise (paratropic: quinoidal) ring currents are indicated by red and blue arrows, respectively. The applied magnetic field is perpendicular to the molecular backbone and pointed out through the molecule plane. ACID plots generated with an isovalue = 0.015 a.u.

the CPDS-CBBT, CPDS-SiBBT, and CPDS-SeBBT polymers show counter-clockwise ring currents, clear clockwise ring currents are visible in the CPDS-NBBT polymer core. This also proves a less quinoidal character in the N substituted polymer compared to the other polymers, which is also validated with BLA, HOMA, NIC-S $_{\rm iso}(1)$, and 2D-ICSS maps as well. Therefore, the substitution of different heteroatoms in the BBT acceptor modulates the local aromatic character of the thiadiazole unit, which leads to aromatic/quinoidal backbones in these polymers. A large quinoidal character of CPDS-CBBT, CPDS-SiBBT, and CPDS-SeBBT facilitates developing large open-shell diradical character in a smaller repeat unit than the CPDS-NBBT polymer.

4 Conclusions

In this work we report novel high-spin ground-state donoracceptor conjugated polymers where the orbital and spin

topologies are modulated by different atomistic substitutions. We utilized the atomistic engineering to tune the aromatic character in the thiadiazole unit of the BBT acceptor. Substitution of different heteroatoms modulates the aromatic/quinoidal nature of the thiadiazole units, which alters the quinoidal character of the polymer's backbone. As a result, the singlettriplet energy gap, the energy gap of the FMOs, open-shell diradical character, and spin and orbital topologies are modulated. The large quinoidal core and aromatic ends accumulate spin densities at the two opposite sides of these polymers. Increasing the oligomer length increases the distance between the unpaired electrons in the polymers' backbone. As a result, the Coulomb repulsion is reduced due to decreased electronelectron repulsion, providing a triplet ground-state at a larger repeat unit. Furthermore, with this simple design strategy, the orbital topologies are modulated from Aufbau to non-Aufbau. The N-substituted CPDS-NBBT polymer with a relatively large aromatic backbone shows Aufbau orbital ordering. However, the C, Si, and

Se substituted polymers with a large quinoidal character show non-Aufbau electronic configurations. These polymers are intriguing synthetic targets for spintronics and room-temperature magnetic materials.

Conflicts of interest

There are no conflicts of interest to declare.

Acknowledgements

This work is supported by the National Science Foundation (NSF) under grant no. OIA-1757220. The DFT calculations were performed at the high-performance computing center at Mississippi State University. Also, the Extreme Science and Engineering Discovery Environment (XSEDE)87 was used, which is supported by NSF grant number ACI-1548562. We acknowledge the Texas Advanced Computing Center (TACC) at the University of Texas at Austin for providing (HPC, Stampede 2 (through XSEDE allocation, TG-CHE140141)) resources that have contributed to the research results reported within this paper. We acknowledge helpful discussions with Prof. Steven Gwaltney at Mississippi State University.

References

- 1 M. Abe, Chem. Rev., 2013, 113, 7011-7088.
- 2 M. Abe, J. Ye and M. Mishima, Chem. Soc. Rev., 2012, 41, 3808-3820.
- 3 M. A. Sabuj and N. Rai, Mol. Syst. Des. Eng., 2020, 5, 1477-1490.
- 4 K. Wang, L. Huang, N. Eedugurala, S. Zhang, M. A. Sabuj, N. Rai, X. Gu, J. D. Azoulay and T. N. Ng, Adv. Energy Mater., 2019, 9, 1902806.
- 5 A. Rajca, Chem. Rev., 1994, 94, 871-893.
- 6 S. Wolf, D. Awschalom, R. Buhrman, J. Daughton, V. S. von Molnár, M. Roukes, A. Y. Chtchelkanova and D. Treger, Science, 2001, 294, 1488-1495.
- 7 L. Bogani and W. Wernsdorfer, Nanoscience And Technology: A Collection of Reviews from Nature Journals, World Scientific, 2010, pp. 194-201.
- 8 M. A. Sabuj, M. M. Huda and N. Rai, iScience, 2020, 23, 101675.
- 9 M. A. Sabuj, Organic Open-Shell Materials for Optoelectronic and Magnetic Applications, Mississippi State University, 2020.
- 10 A. Rajca, Adv. Phys. Org. Chem., 2005, 40, 153-199.
- 11 A. Rajca, M. Takahashi, M. Pink, G. Spagnol and S. Rajca, J. Am. Chem. Soc., 2007, 129, 10159-10170.
- 12 N. M. Gallagher, A. Olankitwanit and A. Rajca, J. Org. Chem., 2015, 80, 1291-1298.
- 13 N. M. Gallagher, J. J. Bauer, M. Pink, S. Rajca and A. Rajca, J. Am. Chem. Soc., 2016, 138, 9377-9380.

- 14 N. Gallagher, H. Zhang, T. Junghoefer, E. Giangrisostomi, R. Ovsyannikov, M. Pink, S. Rajca, M. B. Casu and A. Rajca, J. Am. Chem. Soc., 2019, 141, 4764-4774.
- 15 W. Wang, C. Chen, C. Shu, S. Rajca, X. Wang and A. Rajca, J. Am. Chem. Soc., 2018, 140, 7820-7826.
- 16 G. J. Snyder, J. Phys. Chem. A, 2012, 116, 5272-5291.
- 17 A. Rajca, Nitroxides, Royal Society of Chemistry, 2021, pp. 359-391.
- 18 T. Y. Gopalakrishna, W. Zeng, X. Lu and J. Wu, Chem. Commun., 2018, 54, 2186-2199.
- 19 A. E. London, H. Chen, M. Sabuj, J. Tropp, M. Saghayezhian, N. Eedugurala, B. Zhang, Y. Liu, X. Gu, B. Wong, N. Rai and J. Azoulay, Sci. Adv., 2019, 5, eaav2336.
- 20 M. A. Sabuj, M. M. Huda, C. S. Sarap and N. Rai, Mater. Adv., 2021, 2, 2943-2955.
- 21 T. L. D. Tam, G. Wu, S. W. Chien, S. F. V. Lim, S.-W. Yang and J. Xu, ACS Mater. Lett., 2020, 2, 147-152.
- 22 Z. Zeng, M. Ishida, J. L. Zafra, X. Zhu, Y. M. Sung, N. Bao, R. D. Webster, B. S. Lee, R.-W. Li and W. Zeng, J. Am. Chem. Soc., 2013, 135, 6363-6371.
- 23 L. Huang, N. Eedugurala, A. Benasco, S. Zhang, K. S. Mayer, D. J. Adams, B. Fowler, M. M. Lockart, M. Saghayezhian and H. Tahir, Adv. Funct. Mater., 2020, 1909805.
- 24 P. Karafiloglou, J. Chem. Educ., 1989, 66, 816.
- 25 J. Su, W. Fan, P. Mutombo, X. Peng, S. Song, M. Ondracek, P. Golub, J. Brabec, L. Veis and M. Telychko, Nano Lett., 2020, 21, 861-867.
- 26 G. Gryn'ova, M. L. Coote and C. Corminboeuf, Wiley Interdiscip. Rev.: Comput. Mol. Sci., 2015, 5, 440-459.
- 27 G. Z. Magda, X. Jin, I. Hagymási, P. Vancsó, Z. Osváth, P. Nemes-Incze, C. Hwang, L. P. Biro and L. Tapaszto, Nature, 2014, 514, 608-611.
- 28 M. Slota, A. Keerthi, W. K. Myers, E. Tretyakov, M. Baumgarten, A. Ardavan, H. Sadeghi, C. J. Lambert, A. Narita and K. Müllen, Nature, 2018, 557, 691-695.
- 29 V. Morozov and E. Tretyakov, J. Mol. Model., 2019, 25, 58.
- 30 M. J. Raiti and M. D. Sevilla, J. Phys. Chem. A, 1999, 103,
- 31 H. Guo, Q. Peng, X.-K. Chen, Q. Gu, S. Dong, E. W. Evans, A. J. Gillett, X. Ai, M. Zhang and D. Credgington, Nat. Mater., 2019, 18, 977-984.
- 32 S. Medina Rivero, R. Shang, H. Hamada, Q. Yan, H. Tsuji, E. Nakamura and J. Casado, Bull. Chem. Soc. Jpn., 2021, 94, 989-996.
- 33 T. Sugawara, H. Komatsu and K. Suzuki, Chem. Soc. Rev., 2011, 40, 3105-3118.
- 34 G. Gryn'va and M. L. Coote, J. Am. Chem. Soc., 2013, 135, 15392-15403.
- 35 P. Franchi, E. Mezzina and M. Lucarini, J. Am. Chem. Soc., 2014, 136, 1250-1252.
- 36 B. L. Westcott, N. E. Gruhn, L. J. Michelsen and D. L. Lichtenberger, J. Am. Chem. Soc., 2000, 122, 8083-8084.
- 37 G. Gryn'ova, D. L. Marshall, S. J. Blanksby and M. L. Coote, Nat. Chem., 2013, 5, 474-481.
- 38 Y. Wang, H. Zhang, M. Pink, A. Olankitwanit, S. Rajca and A. Rajca, J. Am. Chem. Soc., 2016, 138, 7298-7304.

- 39 S. M. Quintero, J. L. Zafra, K. Yamamoto, Y. Aso, Y. Ie and J. Casado, J. Mater. Chem. C, 2021, 9, 10727-10740.
- 40 R. Murata, Z. Wang, Y. Miyazawa, I. Antol, S. Yamago and M. Abe, Org. Lett., 2021, 23, 4955-4959.
- 41 J. D. Yuen, R. Kumar, D. Zakhidov, J. Seifter, B. Lim, A. J. Heeger and F. Wudl, Adv. Mater., 2011, 23, 3780-3785.
- 42 J. D. Yuen, J. Fan, J. Seifter, B. Lim, R. Hufschmid, A. J. Heeger and F. Wudl, J. Am. Chem. Soc., 2011, 133, 20799-20807.
- 43 J. Fan, J. D. Yuen, M. Wang, J. Seifter, J.-H. Seo, A. R. Mohebbi, D. Zakhidov, A. Heeger and F. Wudl, Adv. Mater., 2012, 24, 2186-2190.
- 44 Y. Zheng and F. Wudl, J. Mater. Chem. A, 2014, 2, 48-57.
- 45 J. Xiong, N. Eedugurala, Y. Qi, W. Liu, A. R. Benasco, Q. Zhang, S. E. Morgan, M. D. Blanton, J. D. Azoulay and Q. Dai, Sol. Energy Mater. Sol. Cells, 2021, 220, 110862.
- 46 G. L. Gibson, T. M. McCormick and D. S. Seferos, J. Am. Chem. Soc., 2012, 134, 539-547.
- 47 M. Li, L. Kou, L. Diao, Q. Zhang, Z. Li, Q. Wu, W. Lu, D. Pan and Z. Wei, J. Phys. Chem. C, 2015, 119, 9782-9790.
- 48 R. S. Ashraf, I. Meager, M. Nikolka, M. Kirkus, M. Planells, B. C. Schroeder, S. Holliday, M. Hurhangee, C. B. Nielsen and H. Sirringhaus, J. Am. Chem. Soc., 2015, 137, 1314-1321.
- 49 Z. Fei, Y. Han, E. Gann, T. Hodsden, A. S. Chesman, C. R. McNeill, T. D. Anthopoulos and M. Heeney, J. Am. Chem. Soc., 2017, 139, 8552-8561.
- 50 C.-C. Chang, C.-P. Chen, H.-H. Chou, C.-Y. Liao, S.-H. Chan and C.-H. Cheng, J. Polym. Sci., Part A: Polym. Chem., 2013, 51, 4550-4557.
- 51 H. A. Saadeh, L. Lu, F. He, J. E. Bullock, W. Wang, B. Carsten and L. Yu, ACS Macro Lett., 2012, 1, 361-365.
- 52 Y.-J. Hwang, G. Ren, N. M. Murari and S. A. Jenekhe, Macromolecules, 2012, 45, 9056-9062.
- 53 C.-H. Tsai, A. Fortney, Y. Qiu, R. R. Gil, D. Yaron, T. Kowalewski and K. J. Noonan, J. Am. Chem. Soc., 2016, 138, 6798-6804.
- 54 M. Al-Hashimi, Y. Han, J. Smith, H. S. Bazzi, S. Y. A. Algaradawi, S. E. Watkins, T. D. Anthopoulos and M. Heeney, Chem. Sci., 2016, 7, 1093-1099.
- 55 D. Çakal, A. Cihaner and A. M. Önal, J. Electroanal. Chem., 2020, 862, 114000.
- 56 H. Zhang, Y. Guo, Z. Wu, Y. Wang, Y. Sun, X. Feng, H. Wang and G. Zhao, J. Lumin., 2020, 117864.
- 57 A. J. Kronemeijer, E. Gili, M. Shahid, J. Rivnay, A. Salleo, M. Heeney and H. Sirringhaus, Adv. Mater., 2012, 24, 1558-1565.
- 58 Z. Chen, W. Li, M. A. Sabuj, Y. Li, W. Zhu, M. Zeng, C. S. Sarap, M. M. Huda, X. Qiao and X. Peng, et al., Nat. Commun., 2021, 12, 1-10.
- 59 M. J. Frisch, G. W. Trucks, H. B. Schlegel, G. E. Scuseria, M. A. Robb, J. R. Cheeseman, G. Scalmani, V. Barone, G. A. Petersson, H. Nakatsuji, X. Li, M. Caricato, A. V. Marenich, J. Bloino, B. G. Janesko, R. Gomperts, B. Mennucci, H. P. Hratchian, J. V. Ortiz, A. F. Izmaylov, J. L. Sonnenberg, D. Williams-Young, F. Ding, F. Lipparini, F. Egidi, J. Goings, B. Peng, A. Petrone, T. Henderson,

- D. Ranasinghe, V. G. Zakrzewski, J. Gao, N. Rega,
- G. Zheng, W. Liang, M. Hada, M. Ehara, K. Toyota,
- Fukuda, J. Hasegawa, M. Ishida, T. Nakajima,
- Y. Honda, O. Kitao, H. Nakai, T. Vreven, K. Throssell,
- A. Montgomery, Jr., J. E. Peralta, F. Ogliaro,
- M. J. Bearpark, J. J. Heyd, E. N. Brothers, K. N. Kudin,
- V. N. Staroverov, T. A. Keith, R. Kobayashi, J. Normand,
- K. Raghavachari, A. P. Rendell, J. C. Burant, S. S. Iyengar,
- J. Tomasi, M. Cossi, J. M. Millam, M. Klene, C. Adamo,
- R. Cammi, J. W. Ochterski, R. L. Martin, K. Morokuma,
- O. Farkas, J. B. Foresman and D. J. Fox, Gaussian 16 Revision B.01, Gaussian Inc., Wallingford CT, 2016.
- 60 A. D. Becke, J. Chem. Phys., 1993, 98, 1372-1377.
- 61 P. Stephens, F. Devlin, C. Chabalowski and M. J. Frisch, J. Phys. Chem., 1994, 98, 11623-11627.
- 62 D. Feller, J. Comput. Chem., 1996, 17, 1571-1586.
- 63 K. L. Schuchardt, B. T. Didier, T. Elsethagen, L. Sun, V. Gurumoorthi, J. Chase, J. Li and T. L. Windus, J. Chem. Inf. Model., 2007, 47, 1045-1052.
- 64 M. M. Francl, W. J. Pietro, W. J. Hehre, J. S. Binkley, M. S. Gordon, D. J. DeFrees and J. A. Pople, J. Chem. Phys., 1982, 77, 3654-3665.
- 65 J. B. Foresman and Æ. Frisch, Exploring Chemistry with Electronic Structure Methods, Gaussian, Gaussian Inc., Wallingford CT, 3rd edn, 2015.
- 66 L. Noodleman, J. Chem. Phys., 1981, 74, 5737-5743.
- 67 E. D. Glendening, C. R. Landis and F. Weinhold, J. Comput. Chem., 2013, 34, 1429-1437.
- 68 P. v R. Schleyer, M. Manoharan, Z.-X. Wang, B. Kiran, H. Jiao, R. Puchta and N. J. van Eikema Hommes, Org. Lett., 2001, 3, 2465-2468.
- 69 R. Ditchfield, Mol. Phys., 1974, 27, 789-807.
- 70 R. Herges and D. Geuenich, J. Phys. Chem. A, 2001, 105, 3214-3220.
- 71 T. A. Keith and R. F. Bader, Chem. Phys. Lett., 1993, 210, 223-231.
- 72 S. Klod and E. Kleinpeter, J. Chem. Soc., Perkin Trans. 2, 2001, 1893-1898.
- 73 J. Kruszewski and T. Krygowski, Tetrahedron Lett., 1972, 13, 3839-3842.
- 74 T. M. Krygowski and M. K. Cyrański, Chem. Rev., 2001, 101, 1385-1420.
- 75 T. M. Henderson, A. F. Izmaylov, G. Scalmani and G. E. Scuseria, J. Chem. Phys., 2009, 131, 044108.
- 76 T. Stein, H. Eisenberg, L. Kronik and R. Baer, Phys. Rev. Lett., 2010, 105, 266802.
- 77 W. Humphrey, A. Dalke and K. Schulten, J. Molec. Graph., 1996, 14, 33-38.
- 78 Y. Liu, H. Phan, T. S. Herng, T. Y. Gopalakrishna, J. Ding and J. Wu, Chem. - Asian J., 2017, 12, 2177-2182.
- 79 A. Thomas, K. Bhanuprakash and K. K. Prasad, J. Phys. Org. Chem., 2011, 24, 821-832.
- 80 J. D. Yuen, M. Wang, J. Fan, D. Sheberla, M. Kemei, N. Banerji, M. Scarongella, S. Valouch, T. Pho and R. Kumar, J. Polym. Sci., Part A: Polym. Chem., 2015, 53, 287-293.

- 81 W. Wang, L. Ge, G. Xue, F. Miao, P. Chen, H. Chen, Y. Lin, Y. Ni, J. Xiong and Y. Hu, Chem. Commun., 2020, 56, 1405-1408.
- 82 T. Yanai, D. P. Tew and N. C. Handy, Chem. Phys. Lett., 2004, **393**, 51-57.
- 83 J.-D. Chai and M. Head-Gordon, Phys. Chem. Chem. Phys., 2008, 10, 6615-6620.
- 84 J. J. Dressler, M. Teraoka, G. L. Espejo, R. Kishi, S. Takamuku, C. J. Gómez-Garca, L. N. Zakharov, M. Nakano, J. Casado and M. M. Haley, Nat. Chem., 2018, 10, 1134-1140.
- 85 G. E. Rudebusch, J. L. Zafra, K. Jorner, K. Fukuda, J. L. Marshall, I. Arrechea-Marcos, G. L. Espejo, R. P. Ortiz, C. J. Gómez-Garca and L. N. Zakharov, Nat. Chem., 2016, 8, 753-759.
- 86 M. Nakano, Excitation energies and properties of open-shell singlet molecules: applications to a new class of molecules for nonlinear optics and singlet fission, Springer, 2014.
- 87 J. Towns, T. Cockerill, M. Dahan, I. Foster, K. Gaither, A. Grimshaw, V. Hazlewood, S. Lathrop, D. Lifka and G. D. Peterson, et al., Comput. Sci. Eng., 2014, 16, 62-74.